ELSEVIER

Journal of Alloys and Compounds 452 (2008) 241–244

Journal of ALLOYS AND COMPOUNDS

www.elsevier.com/locate/jallcom

Superconductivity and physical properties of a LaRhSn single crystal

Matúš Mihalik [a], Vladimír Sechovský [a,*], Martin Diviš [a], Slavomír Gabáni [b], Marián Mihalik [b]

[a] *Charles University, Faculty of Mathematics and Physics, Department of Condensed Matter Physics, Ke Karlovu 5, 121 16 Prague 2, Czech Republic*

[b] *Slovak Academy of Sciences, Institute of Experimental Physics, Watsonova 47, 04001 Košice, Slovakia*

Received 10 December 2006; received in revised form 22 January 2007; accepted 23 January 2007
Available online 28 January 2007

Abstract

Single crystals of LaRhSn have been grown and studied with respect to the electrical resistivity and specific heat, which were measured in the temperature range from 0.1 to 300 K in various magnetic fields. The compound was found to be superconducting at temperatures lower than $T_c = 1.85 \pm 0.05$ K. The critical field B_{c2} and also the temperature dependence $B_{c2}(T)$ were found to be dependent on the geometry of the experiment with respect to the direction of the magnetic field (applied along the *a*- or *c*-axis). The electrical resistivity measurements at temperatures higher than 2 K revealed metallic behavior with a considerable anisotropy between the *a*-axis and the *c*-axis. The experimental results are also discussed in the light of our *ab initio* electronic-structure calculations.

PACS: 74.70.Dd; 74.25.Fy; 74.25.Bt; 71.15.Mb

Keywords: Intermetallics; Superconductors; Heat capacity; Electrical resistivity

1. Introduction

In recent years, there has been a great deal of interest in the study of rare-earth containing intermetallic compounds of the type RTX, where R is a rare-earth element, T and X is a d- and a p-metal, respectively. These compounds crystallize in a variety of structure types, depending on the T and X element species and exhibit various interesting physical properties. The most attractive are superconductivity with the critical temperature around 2 K (LaRhSn [1] and LaRhSb [2]), Kondo behavior (CeNiSn [3] and CeRhSb [4]) and non-Fermi-liquid behavior (CeRhSn [5]). Numerous Sn-containing compounds exhibit antiferromagnetic ordering of rare-earth magnetic moments (NdNiSn [6], CePdSn [7] and other compounds) whereas many compounds with Sb order ferromagnetically (for example NdNiSb [8], PrPdSb [9]).

LaRhSn crystallizes in the hexagonal ZrNiAl-type structure (space group $P\bar{6}2m$). First, electrical resistivity and ac susceptibility measurements on polycrystalline LaRhSn sample revealed superconducting phase with the critical temperature $T_c = 1.7$ K [10]. Next Ho et al. studied also polycrystalline samples and reported $T_c = 2$ K and the critical field for destroying superconductivity rising from 0.1 T at 1.6 K to 0.7 T at 0.2 K [1]. It is worth to note that the magnetic susceptibility of LaRhSn in the normal state is remarkably higher than the susceptibility of CeRhSn [11]. Up to now a LaRhSn single crystal was studied only as a nonmagnetic analogue within investigation of the CeRhSn compound [5]. Since the superconducting transition in LaRhSn was studied so far only on polycrystalline samples [1] we decided to grow a single crystal and to study the specific heat and electrical resistivity near the critical temperature T_c. To understand the behavior of LaRhSn more closely we performed also *ab initio* calculations of electronic structure of this compound and discuss the results of calculations together with experimental data.

2. Experimental and calculation details

Two single crystals (i) and (ii) of LaRhSn have been grown by a modified Czochralski method in a tri-arc furnace under purified Ar atmosphere from a melt

* Corresponding author.
E-mail address: sech@mag.mff.cuni.cz (V. Sechovský).

0925-8388/$ – see front matter © 2007 Elsevier B.V. All rights reserved.
doi:10.1016/j.jallcom.2007.01.121

consisting of the stoichiometric composition of the high purity (La: 99.9%; Rh: 99.9; Sn: 99.8) element metals using a tungsten rod as a seed. The quality of the crystals was checked and confirmed by Laue patterns. Rietveld analysis of the X-ray powder diffractogram revealed only the LaRhSn phase within the sensitivity of the method. The lattice parameters of both single crystals were found identical ($a = 0.7479(3)$ nm; $c = 0.4217(4)$ nm; $x_{La} = 0.591(4)$ and $x_{Sn} = 0.243(8)$) and are in good agreement with data published by Slebarski et al. [11].

Temperature dependences of the specific heat (C) and electrical resistivity (ρ) were measured with the PPMS (Quantum Design) apparatus using a ^{3}He insert for cooling below 2 K. We used the crystal (ii) for these measurements. The electrical resistivity was measured by a standard four-probe ac method with driving current of 500 μA. The experimental error for measuring the voltage on the sample was less than 4%. The temperature of superconducting transition T_c in all experiments (with and without magnetic field) was determined with the temperature at which the resistivity drops to zero.

The specific heat was measured by the relaxation method described in Ref. [12] with the error less than 3% for temperatures lower than 2 K (He3 insert) and less than 1% for $T > 2$ K.

The critical field (B_{c2}) was studied on both the crystals (i) and (ii) in the Oxford TLE-200 ^{3}He^{4}He dilution refrigerator and was determined as a field in which the maximum slope of the $\rho(B)$ dependence at constant temperature was observed. Temperature was measured by a calibrated germanium Lake Shore sensor GR-200A-50. In this experiment the driving current was 100 μA.

The electronic structure was calculated in the framework of the density functional theory (DFT). We have used both the local density approximation (LDA) [13] and the generalized gradient approximation (GGA) [14]. The Kohn–Sham equations of DFT were solved using full potential augmented plane wave plus local orbitals (APW + lo) WIEN2k code [15]. The relativistic effects were treated in the scalar relativistic approximation [16]. Atomic sphere (AS) radii of 2.5, 2.3 and 2.1 Bohr radii (1 Bohr = 52.9177 pm) were chosen for La, Rh and Sn, respectively. We have used a basis of about 1450 APW functions (about 160 per atom) in the interstitial region and the maximum $l = 12$ in the expansion of the radial wave functions inside the AS to represent the valence states. Local orbitals were used to treat the fully occupied La-5s-5p, Rh-4s-4p and Sn-4p-4d states with the valence states in a single energy window. The advantage of this treatment is that the above-mentioned semicore states are orthogonal to the valence states. Both the potential and the charge density were expanded inside the AS into crystal harmonics up to $L = 6$ and in the interstitial region into a Fourier series with about 5793 K stars. For the Brillouin zone (BZ) integration, a modified tetrahedron method [15] with 198 special k-points in the irreducible wedge (2000 k-points in the full BZ) was used to construct the charge density in each self-consistency step. We have carefully checked that with these parameters the calculations converge. The values of the internal structure parameters x_{La} and x_{Sn} were obtained by minimizing the forces for fixed values a and c determined from experiment. Such calculated values of the free internal parameters are close to the values determined from the experiment.

We also wanted to compare the performance of LDA and GGA with respect to the equilibrium volume of LaRhSn. The experimental c/a ratio and the symmetry-free structure parameters obtained from minimization of the forces were used and kept constant during the calculations. The LDA value of the equilibrium volume is smaller comparing the experimental value by about 4.6%. This is a typical deviation usually obtained in LDA calculations. The GGA, on the other hand, overestimated experimental V_0 by only 2.3%, so the GGA provides a better equilibrium volume than LDA.

3. Results

The specific heat of LaRhSn (Fig. 1.) exhibits a lambda anomaly and reaches the maximum value $C_s = 0.0485$ J mol^{-1} K^{-1} at $T_c = 1.85 \pm 0.05$ K. Taking into resistivity data discussed below we attributed the $C(T)$ peak to the transition from the normal to the superconducting state. When a magnetic field is applied along the c-axis the $C(T)$ anomaly moves to lower temperatures and becomes reduced. Finally, in the field of 0.3 T field the peak is no more indicated in the temperature

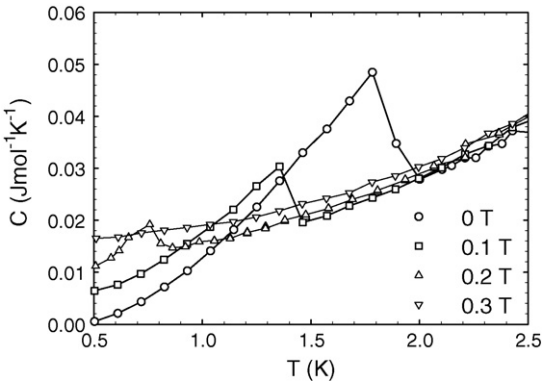

Fig. 1. A low temperature detail of the temperature dependence of the specific heat of the crystal (ii) of LaRhSn, which shows evolution of the superconducting transition with respect to the magnetic field applied along the c-axis. The lines are only guides for the eye.

range (0.5–300 K) of our measurement on PPMS. At $T_c = 1.85$ (zero-field value) the sample in the field of 0.1 T is still in the normal state and the specific heat amounts only the value $C_n = 0.0243$ J mol^{-1} K^{-1}. Then the ratio $(C_s - C_n)/C_n \cong 1$ is much lower than the value of 1.43 predicted by BCS theory.

In the temperature range 2–8 K the specific heat data fit with the equation $C = \gamma T + \beta T^3$, where γT and βT^3 describe the electronic and phonon contributions to the specific heat, respectively, with the parameters $\gamma = 10.9$ mJ mol^{-1} K^{-2} and $\beta = 6.2 \times 10^{-4}$ J mol^{-1} K^{-4}. From our first principles band structure calculations based on the density functional theory we have obtained $\gamma_{DFT} = 6.68$ mJ mol^{-1} K^{-2} by the GGA method. The calculated Fermi level is situated at a peak in the density of states (DOS) (see Fig. 2). The DOS at Fermi level leads to enhancement factor $\lambda = 0.63$ with λ defined by $\gamma = \gamma_{DFT}(1 + \lambda)$.

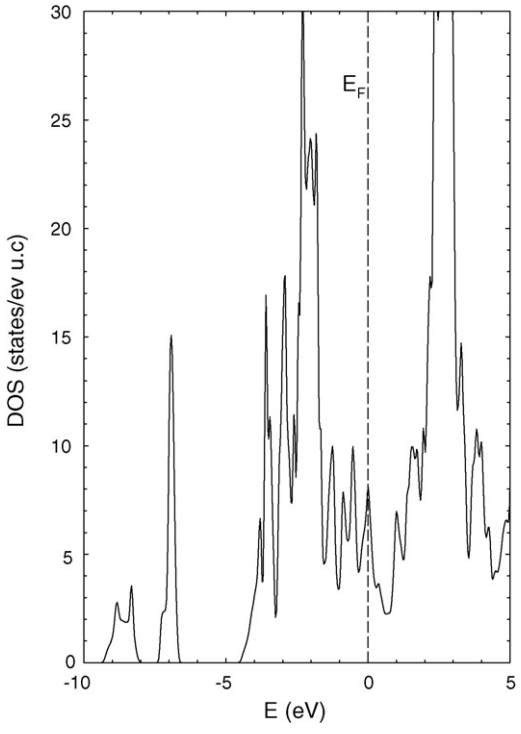

Fig. 2. The density of states curve calculated for the LaRhSn compound.

The entire enhancement is most likely due to the electron-phonon coupling. Using McMillan formula [17] one obtains $T_c = 3.34$ K which is a reasonable estimate of the superconducting temperature of the LaRhSn. The complex band structure of LaRhSn suggests the multiband nature of the superconductivity, which cannot be accounted by a simple BCS theory. Using equation:

$$\beta = \frac{12}{5}\pi^4 N \frac{R}{\theta_D^3}$$

where R is a gas constant, N the number of atoms per formula unit and θ_D is a Debye temperature we can estimate $\theta_D = 211$ K. Below T_c the specific heat can be fitted by:

$$C = \beta T^3 + c e^{-\Delta/T}$$

where the first term is due to the phonon contribution and the second term is associated with the energy gap between normal and superconducting state. This equation differs from dependency predicted by BCS theory by a prefactor $1/T^{3/2}$. During the fit we have fixed β to the value obtained from fit in the normal state. We have obtained a fine fit (Fig. 3) for temperatures lower than 1.8 K with coefficients $c = 0.23$ J mol^{-1} K^{-1} and $\Delta = 3$ K.

The relative resistivity (measured on the crystal (ii)) shows metallic behavior. The a-axis resistivity as about double of that measured for current along the c-axis. The residual resistivity ratio for current applied along both the axes is about 7.5. At low temperatures the resistivity drops to zero value at $T_c = 1.9$ K (Figs. 4 and 5). This drop clearly indicates that LaRhSn is superconducting below T_c. When a magnetic field is applied along the current direction the superconducting transition shifts to lower temperatures (Figs. 4 and 5) and finally in fields higher than 0.2 T the T_c appears below the low-temperature limit of this experiment (0.5 K). The additional study of $B_{c2}(T)$ dependences performed on both crystals in a ^{3}He^{4}He dilution refrigerator and for both crystallographic directions revealed considerably different behavior between the configurations ($I \| a$, $B \| c$) and ($I \| c$, $B \| a$) (Fig. 6). For the field applied along the c-axis and the electrical current along the a-axis the $B_{c2}(T)$ values increase nearly linearly with decreasing temperature with $B_{c2} \approx 0.5$ T at $T = 0.1$ K. In this case the shape of $B_{c2}(T)$ curve is rather sample-independent. These agrees well with $B_{c2}(T)$ data (also plotted in Fig. 6) derived from the $\rho(T)$ results mentioned above, which were collected on sample (ii) in various magnetic fields parallel to current directions ($I \| a$, $B \| a$) and ($I \| c$, $B \| c$).

Strikingly different results were, however, obtained on both samples for the magnetic field applied along the a-axis and electrical current applied along the c-axis. In this case the $B_{c2}(T)$

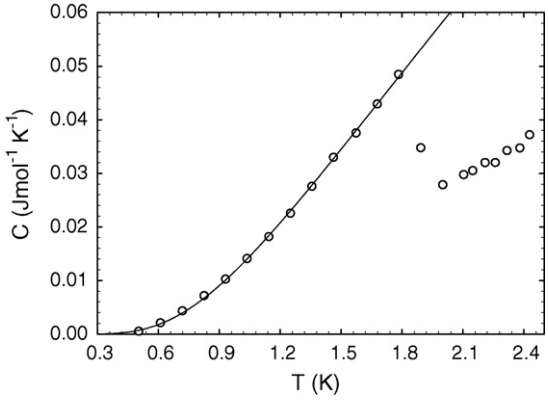

Fig. 3. Comparison of specific heat data in the superconducting state with the fit (see text).

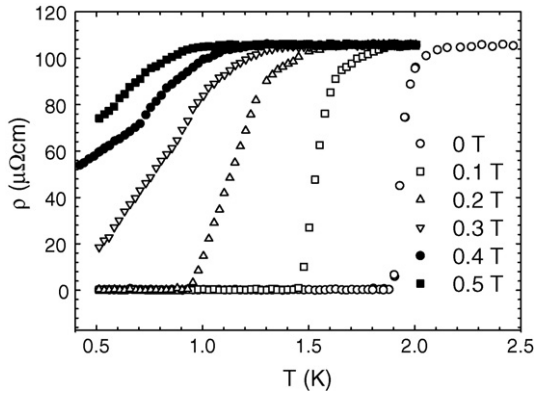

Fig. 4. The temperature dependence of the electrical resistivity of the crystal (ii) of LaRhSn near the superconducting transition in magnetic fields for the magnetic field and electrical current applied along the a-axis.

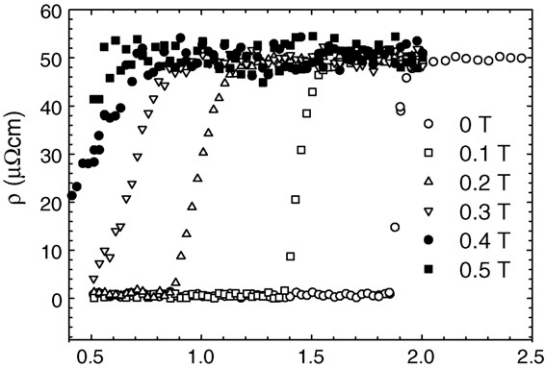

Fig. 5. The temperature dependence of the electrical resistivity of the crystal (ii) of LaRhSn near the superconducting transition in magnetic fields for the magnetic field and electrical current applied along the c-axis.

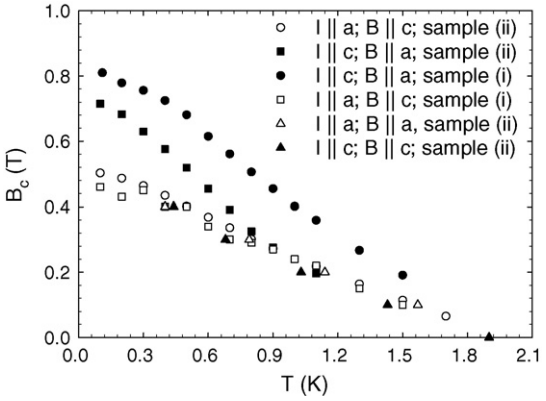

Fig. 6. The critical magnetic field B_{c2} as a function of temperature determined for LaRhSn. Circles and squares were derived from the field dependences of the resistivity at constant temperature and the triangles were derived from the temperature dependence of the resistivity at a fixed magnetic field.

curves show tendency to saturate below 0.4 K and also show sample dependent values of the critical field $B_{c2} \approx 0.7$ T (sample (i)) or $B_{c2} \approx 0.8$ T (sample (ii)) both taken at $T = 0.1$ K. These values rather corresponds to results obtained on a polycrystalline sample by Ho et al. [1], however are much higher than corresponding data on our single crystal in case of $B \| c$-axis. In this stage of the research, however, we have no plausible explanation for this result. Further experimental activities on new high-quality crystals will be attempted in order to resolve the problem.

4. Conclusions

By specific heat and resistivity measurements we have confirmed superconductivity in LaRhSn single crystals below the critical temperature $T_c = 1.85 \pm 0.05$ K. A considerably sharper transition from the normal state to the superconducting state was observed on the temperature dependence of the electrical resistivity measured for current applied along the c-axis ($I \| c$) in comparison to data measured for $I \| a$-axis. Our study also revealed quite different behavior of $B_{c2}(T)$ between the current–magnetic field configurations ($I \| a$, $B \| c$) and ($I \| c$, $B \| a$). The critical field B_{c2} increases nearly linearly with decreasing temperature in the ($I \| a$, $B \| c$) configuration reaching the value $B_{c2} \approx 0.5$ T at $T = 0.1$ K. In the ($I \| c$, $B \| a$) configuration the $B_{c2}(T)$ curves have tendency to saturate below 0.4 K and depending on the sample the critical field $B_{c2} \approx 0.7$ T or $B_{c2} \approx 0.8$ T at $T = 0.1$ K, which are much higher values than the value obtained for first one configuration. The origin of the observed anisotropy of the $B_{c2}(T)$ behavior with respect to direction of applied magnetic field is not yet understood and further experimental effort on this material is therefore desirable.

Specific-heat data indicate that the superconductivity in LaRhSn cannot be explained within the simple BCS theory of superconductors, which agrees with the complex nature of the calculated electronic structure of LaRhSn.

Acknowledgements

This work is a part of the research program MSM 0021620834 financed by the Ministry of Education of the Czech Republic. Measurements performed in ^{3}He^{4}He dilution refrigerator were supported by Center of Excellence of the SAS, Contract No. I/2/2003 and APVT 51-031704 project.

References

[1] P.-C. Ho, V.S. Zapf, A. Slebarski, M.B. Maple, Philos. Mag. 84 (2004) 2119.
[2] S.K. Malik, H. Takeya, K.A. Gschneider, Phys. Rev. B 50 (1994) 12540.
[3] M. Kasaya, T. Tani, F. Iga, T. Kasuya, J. Magn. Magn. Mater. 76–77 (1988) 278.
[4] B.D. Rainford, D.T. Adroja, J.M.E. Geers, Phys. B 199–200 (1994) 556.
[5] M.S. Kim, Y. Echizen, K. Umeo, S. Kobayashi, M. Sera, P.S. Salamakha, O.L. Sologub, T. Takabatake, X. Chen, T. Tayana, T. Sakakibara, M.H. Jung, M.B. Maple, Phys. Rev. B 68 (2003) 054416.
[6] A. Szytula, B. Penc, N. Stűsser, J. Magn. Magn. Mater. 265 (2003) 94.
[7] M. Kasaya, T. Tani, K. Ohoyarna, M. Kohgi, Y. Isikawa, J. Magn. Magn. Mater. 104–107 (1992) 665.
[8] I. Karla, J. Pierre, A.P. Murani, M. Neumann, Phys. B 271 (1999) 294.
[9] D.T. Adroja, B.D. Rainford, S.K. Malik, H. Takeya, K.A. Gschneidner Jr., V.K. Pecharsky, J. Alloys Comp. 288 (1999) 7.
[10] F. Canepa, S. Cirafici, J. Alloys Comp. 232 (1996) 71.
[11] A. Slebarski, M. Radlowska, T. Zawada, M.B. Maple, A. Jezierski, A. Zygmunt, Phys. Rev. B 66 (2002) 104434.
[12] J.S. Hwang, K.J. Lin, Ch. Tien, Rev. Sci. Instrum. 68 (1997) 94.
[13] J.P. Perdew, Y. Wang, Phys. Rev. B 45 (1992) 13244.
[14] J.P. Perdew, S. Burke, M. Ernzerhof, Phys. Rev. Lett. 77 (1996) 3865.
[15] P. Blaha, K. Schwarz, G. Madsen, D. Kvasnicka, J. Luitz, in: K. Schwarz (Ed.), WIEN2k, an Augmented Plane Wave + Local Orbitals Program for Calculating Crystal Properties, TU Wien, Austria, 2001. ISBN 3-9501031-1-2.
[16] D.D. Koelling, B.N. Harmon, J. Phys. C: Solid State Phys. 10 (1977) 3107.
[17] W.L. McMillan, Phys. Rev. 167 (1968) 331.